THE SUPPLY OF NUTRIENTS DUE TO VERTICAL TURBULENT MIXING: A STUDY AT THE PORCUPINE ABYSSAL PLAIN STUDY SITE (49ºN 16º30'W) IN THE NORTHEAST ATLANTIC

Adrian P. Martin[a,*], Michael I. Lucas[a], Stuart C. Painter[a], Rosalind Pidcock[a], Hartmut Prandke[b], Holger Prandke[b], Mark C. Stinchcombe[a]

[a] National Oceanography Centre, Southampton, SO14 3ZH, UK

[b] ISW Wassermesstechnik, Lenzer Strasse 5, OT Petersdorf, D - 17213 Fünfseen, Germany

* Corresponding author. Tel.: 00 44 (0)23 80596342; Fax: 00 44 (0)23 80596247; email: apm1@noc.soton.ac.uk

Abstract

As part of a multidisciplinary cruise to the Porcupine Abyssal Plain (PAP) study site (49º00'N 16º30'W), in June and July of 2006, observations were made of the vertical nitrate flux due to turbulent mixing. Daily profiles of nitrate and turbulent mixing, at the central PAP site, give a mean nitrate flux into the euphotic zone of 0.09 (95% confidence intervals: 0.05-0.16) mmol N m^{-2} d^{-1}. This is a factor of fifty lower than the mean observed rate of nitrate uptake within the euphotic zone (5.1+/-1.3 mmol N m^{-2} d^{-1}). By using our direct observations to 'validate' a previously published parameterisation for turbulent mixing we further quantify the variability in the vertical turbulent flux across a roughly 100 km x 100 km region centred on the PAP site, using hydrographic data. The flux is uniformly low (0.08 +/- 0.26 mmol N m^{-2} d^{-1}, the large standard deviation being due to a strongly non-Gaussian distribution) and is consistent with direct measurements at the central site. It is demonstrated that on an annual basis convective mixing supplies at least forty-fold more nitrate to the euphotic zone than turbulent mixing at this location. Other processes, such as those related with mesoscale phenomena, may also contribute significantly.

1. Introduction

It may be thought surprising to claim that phytoplankton, upon whom so much life in the sea depends, live on the margins of the open ocean. Yet they are typically confined to the upper 100m of a water column which extends to 4km or more. This edge existence arises from the rapid absorption by water of the sunlight phytoplankton need to photosynthesise. This would not be a problem for survival if they did not also need nutrients to grow. However, the majority of nutrients used by phytoplankton arise from the regeneration of decaying organic material and gravity ensures that this process of nutrient recycling and accumulation occurs at depth. For phytoplankton to grow it is therefore necessary to bring deep waters laden with nutrients to the surface – a role fulfilled by the ubiquitous advection and mixing of water. Without this physical 'supply line', phytoplankton in the open ocean would be much less abundant and the dominant species very different. The small oligotrophy specialist phytoplankton would dominate and even nitrogen fixers would find it difficult to thrive due to the high N:P of atmospheric deposition.

The role of the physical circulation in controlling phytoplankton abundance and productivity has been recognised for some time and a multitude of mechanisms have been identified. Winter convective mixing (Williams et al., 2000), mesoscale upwelling (Pollard & Regier, 1992; Allen et al., 2005) and small-scale turbulent mixing (Lewis et al., 1986; Carr et al., 1995; Law et al., 2001; Law et al., 2003) are three that have received perhaps the most attention. To understand the controls on phytoplankton growth in a region, it is necessary to quantify the contributing flux associated with each pathway. These contributions all vary in time and space. Winter mixing stirs large quantities of nutrients to the surface but does so only for a relatively short period each year. Mesoscale processes work throughout the year, but, though

56 they may drive large fluxes, they are intermittent in space and time. Though
57 turbulence at scales from centimetres to metres is also intermittent in space and time,
58 these scales are so much smaller than those involved in mesoscale processes that such
59 fluctuations in the circulation can be viewed as a constant background effect. For this
60 reason, their cumulative effect is often modeled by analogy to molecular diffusion:
61 there too, intermittent displacements of varying size nevertheless result in dispersion
62 at larger scales. Accordingly, mixing due to these small-scale processes is often
63 referred to as turbulent diffusivity, even though it is unrelated to (and much larger in
64 magnitude than) molecular diffusivity.

65 The turbulent diffusivity is typically $10^{-2}m^2s^{-1}$ or more in the mixed layer but
66 several orders of magnitude smaller deeper down (see for example Ledwell et al.,
67 1998; Polzin et al., 1997). This reflects the major contribution of atmospheric cooling
68 and wind-driven mixing to surface mixing with deeper turbulent motion being driven
69 by processes such as breaking internal waves and interactions with topography.

70 We focus here on the turbulent flux of nitrate. We do this despite having
71 equivalent measurements for phosphate and silicate concentrations. The reason for
72 this choice is that we have simultaneous measurements for nitrate uptake. Therefore,
73 for nitrate it is possible to put the turbulent flux in context with the observed rate of
74 the nutrient's uptake by phytoplankton.

75 There are relatively few direct measurements of the nitrate flux due to
76 turbulent mixing in the open ocean. In the Southern Ocean, Law et al. (2003) found
77 the turbulent flux to account for just 8% of the nitrate required for observed carbon
78 fixation rates. Naveira-Garabato et al. (2002) also found it to be a minor flux in the
79 Antarctic Polar Front. In the northern North Atlantic, the flux accounted for just 16%
80 of the observed drawdown of nitrate during a summer cruise (Law et al., 2001). In the

equatorial Pacific, Carr et al. (1995) found that vertical turbulent mixing could account for roughly a third of the nitrate drawdown between 0 and 2ºS but was a negligible contributor further away from the equator. As the turbulent nitrate flux is always present, it may be thought that it would be most significant in oligotrophic regions, particularly during the stratified summer, where open ocean phytoplankton are often nutrient limited. In the subtropical Atlantic Lewis et al. (1986) did indeed find the turbulent supply to match the rate of nitrate uptake. However, the measurements of nitrate uptake were substantially smaller than estimates arising from tracer methods (e.g. Jenkins and Doney, 2003). There is, furthermore, little knowledge concerning how vertical turbulent mixing varies at the mesoscale (Naveira-Garabato et al., 2002). This is despite the long-standing paradigm that such mixing may be strongly influenced by vertical gradients in horizontal currents, or shear (see for example Turner, 1973). As mesoscale features such as eddies and fronts display strong heterogeneity in shear, it is germane to ask if rates of turbulent mixing also vary on these scales, with significantly higher mixing in regions of high strain. It might be anticipated that turbulent mixing may vary considerably over a region large enough to encompass varying strengths of mesoscale activity.

We present measurements of the vertical nitrate flux due to small-scale turbulent mixing at the Porcupine Abyssal Plain (PAP) study site at 49º00'N16º30'W in the Northeast Atlantic. The data were obtained as part of the D306 cruise from 23 June to 8 July 2006 on board RRS Discovery. It comprised a daily suite of measurements at the PAP site augmented by a high resolution physical survey spanning the last 4 days of the cruise and sampling a region roughly 100 km x 100 km (Figure 1). The latter was intended to delineate the mesoscale physical structure and variability of the region.

We provide direct estimates of the turbulent nitrate flux into the euphotic zone in this area. This is achieved using observations from turbulence profiles carried out immediately subsequent to CTD casts from which water was collected for nutrient analysis. These flux estimates are compared with concurrent, and co-located, observations of the rate of nitrate uptake. Preliminary results on the mesoscale variability of the turbulent flux of nitrate are also presented. We test the applicability of published parameterisations of turbulent diffusivity (which use current shear and buoyancy frequency to make predictions) and use the most accurate for our region to estimate the mesoscale variability of the turbulent nitrate flux using physical hydrographic data from the mesoscale survey. We are, to the best of our knowledge, the first to use direct measurements to 'validate' a parameterisation for estimating the turbulent diffusivity before applying it to determine mesoscale spatial variability in the turbulent flux of nutrients for the open ocean.

The structure of the paper is as follows. Following this introduction, in Section 2, we describe the various methods, including those used to measure turbulent mixing, nitrate concentrations and uptake and mesoscale variability in physical structure. In Section 3 we present our results, both for a comparison of turbulent nitrate supply to nitrate uptake at the central PAP site and for the mesoscale variability of the flux. A discussion of our results is found in Section 4 prior to our conclusions in Section 5.

2. Methods

The central measurement for this study is the vertical turbulent flux of nitrate. It has already been stated that the conventional model for this physical process is by direct analogy with molecular diffusion. For this reason, the changes in distribution of an

inert tracer *C* undergoing turbulent mixing are modeled, in the standard Fickian manner, as

$$\frac{\partial C}{\partial t} = \frac{\partial}{\partial z}\left(\kappa(z)\frac{\partial C}{\partial z}\right) \quad (1)$$

where *t* is time, *z* is depth and κ is the turbulent, or effective, diffusivity. We are interested in the supply of nitrate, *N*, to the surface. Since the turbulent flux is zero at the surface, by integrating over depth we obtain the rate at which nitrate is entering that portion of ocean through its lower boundary,

$$F(d) = \kappa(z)\frac{\partial N}{\partial z}\bigg|_{z=d} \quad (2)$$

i.e. the rate of supply of nitrate via turbulent mixing to the water above depth *d* is the product of the turbulent diffusivity and the nitrate gradient at depth *d*. Therefore, to estimate *F(d)* we simply require vertical profiles for both nitrate and κ.

2.1 Turbulent diffusivity measurements

The microstructure profiler used to measure turbulent diffusivities (MSS90L, serial number 10) was produced by Sea and Sun Technology GmbH in co-operation with ISW Wassermesstechnik. The latter participated in the cruise and carried out the measurements.

The profiler is equipped with two velocity microstructure shear sensors as well as standard high precision conductivity, temperature, depth (CTD) sensors. The sampling rate for all sensors is 1024 samples per second, with 16 bit resolution. Although it is attached to the ship by a cable (providing power and data transmission), the profiler is allowed to sink in freefall by maintaining sufficient slack cable in the water at all times. This is to minimise contamination of the signal by vibrations of the

profiler caused by tension in the cable. All sensors are mounted at the measuring head of the profiler with the microstructure sensors placed at the tip of a slim shaft, about 150mm in front of the CTD sensors. This minimises contamination of any signal by turbulence created by the profiler itself sinking through the water. A vibration control sensor and a two component tilt sensor also provide data to remove noise contamination from the signal. The general behaviour of the MSS profiler is described in detail by Prandke et al. (2000). The calibration of the CTD sensors was carried out by Sea & Sun Technology GmbH using standard calibration equipment and procedures for CTD probes. The vibration control sensor, the tilt sensors and the shear sensors were calibrated by ISW Wassermesstechnik.

The turbulent energy dissipation rate in 1 m depth bins has been estimated following $\varepsilon = 7.5 \cdot \nu \overline{(\partial u / \partial z)^2}$ where ν is the kinematic viscosity and $\partial u / \partial z$ is the small-scale current shear. The processing of the shear data has been carried out as described by Prandke (2005). The turbulent diffusivity is then calculated from the dissipation rate using $\kappa = \gamma \cdot \varepsilon / N^2$ (Osborn, 1980) where N is the buoyancy frequency and γ is the mixing efficiency. A constant mixing efficiency of 0.2 was used.

Each deployment of the profiler comprised a number of profiles. This is necessary because the mixing processes involved are intermittent such that consecutive profiles often show considerably different, yet genuine, structure. It is therefore advisable to combine several profiles for each deployment to calculate a mean profile of turbulent diffusivities. Analysis of the diffusivities at the same depth for different profiles of the same deployment revealed a strongly non-Gaussian distribution. The observations fitted a log-normal distribution for nearly all depths and deployments when tested using a Kolmogorov-Smirnov test on the log-transformed data. Given the relatively small number of profiles per deployment (between 5 and

179 10) we therefore followed the Baker and Gibson (1987) method for estimating the
180 mean diffusivity. More specifically the mean is estimated as $M=\exp(m+v^2/2)$ where m
181 and v^2 are the mean and variance of the log-transformed data respectively and the
182 95% confidence intervals are given by $M*\exp(+/-1.96*\eta)$ where $\eta=\sqrt{[v^2/n+v^4/2(n-1)]}$
183 and n is the number of data points. For this averaging process data were further
184 averaged in 4 dbar bins. Estimates formed in this way are consistently less noisy than
185 those obtained by naively using the arithmetic mean. This is by simple virtue of the
186 latter method being more strongly influenced by outlying large values. For all but a
187 few points very near to the surface the Thorpe length is less than 4m. Therefore, the
188 size of the overturns comprising the turbulence is smaller than the scale of vertical
189 averaging.
190
191 *2.2 Nitrate measurements*
192
193 Throughout the paper, nitrate represents the sum of nitrate and nitrite. Samples for
194 analysis were drawn directly into 25 ml plastic coulter counter vials from Niskin
195 bottles that had been lowered on the CTD frame. The vials were stored in the dark at
196 4^oC until analysis, which commenced within 24 hours of sampling. Nitrate was
197 determined in unfiltered water samples with a Skalar Sanplus segmented flow
198 autoanalyser and standard colorimetric techniques described by Kirkwood (1995) and
199 Sanders et al. (2007).
200 Overall, the precision of the data is estimated to be better than ± 0.12 μmol l^{-1}
201 (0.6 % of the top standard). Consistency of the data was ensured by the analysis of
202 commercial nutrient standards (Ocean Scientific International, Petersfield, Hants,

UK). Concentrations of nutrients determined in the commercially available nutrient standards were within 4% of their designated values.

The consistency in the vertical profile of nitrate throughout the cruise was remarkable (Fig 2a). This is despite strong evidence for advection of spatial variability through the site (Painter et al., 2008b). It was therefore possible to construct a statistical model to provide estimates of nitrate concentration for the mesoscale survey where nitrate was only sampled at a subset of points. Predictions of nitrate, N_{pred}, from the model (fitted by minimising the least squares difference between predictions and observations using the simplex algorithm – see for example Press et al., 1992)

$$N_{pred} = A * \frac{P^B}{C + P^B},$$

where P is pressure in dbar, A= 14.5135 mmol N m^{-3}, B= 1.1131 and C= 143.1686 $(dbar)^B$, are correlated with observations with R^2=0.91 (Fig 2b)[1]. It is, therefore, a good first approximation to use the statistical model's vertical profile of nitrate to calculate the turbulent nitrate flux at different locations within the mesoscale survey area.

2.3 Nitrate uptake measurements

Sample water recovered from 6 light depths (97, 55, 33, 14, 4.5, 1%) was decanted directly into duplicated new 2 l acid-washed Nalgene polycarbonate incubation bottles for each light depth. One of these bottles was darkened with tin-foil and black tape to serve as a control for dark nitrate uptake. All bottles containing exactly 2 l sample water were inoculated with 100-200 µl stock solution of $K^{15}NO_3^-$ (1

[1] It is worth noting in passing that an ISUS nitrate sensor was deployed on many of the CTD casts from which water was drawn for nitrate samples. However, perhaps by virtue of the very stable vertical structure, the ISUS data were much worse predictors of nitrate concentration than the above simple pressure-based model. For that reason the latter is used here. Subsequent work may have improved the accuracy and precision of ISUS (Sakamoto et al., 2008).

μmol / 100 μl), the volume of ^{15}N spike being adjusted to ~10% of the ambient NO_3^- concentration.

After spiking, the incubation bottles were transferred to Perspex incubation tubes covered with neutral density filters (Lee: Misty Blue [061] and Neutral Density Grey [210 ND]) that re-constructed water column light attenuation (97, 55, 33, 14, 4.5 and 1% incoming irradiance) and removed red light. The incubators were cooled by a constant flow of surface seawater.

At the end of the ~10 hr incubation period, all ^{15}N incubations were filtered onto 25 mm ashed Whatman GF/F filters that were then stored at –20 ˚C for later analysis by stable isotope mass spectrometry on the NOC's Stable Isotope Ratio Mass Spectrometry facility (NOC's-SIRMS) using a Eurovector elemental analyser coupled to a GV Isoprime mass spectrometer. The calibration standard was tyrosine, traceable to International Atomic Energy Agency standards. Nitrate uptake was calculated according to Dugdale and Goering (1967) and Dugdale and Wilkerson (1986) using particulate N concentrations measured at the end of the incubation to account for unlabelled N.

A standard astronomical formula was used to calculate the duration of daylight hours for the year day and position. The uptakes in light and dark bottles were then combined in a ratio equal to that of daylight hours to night-time hours to give the daily average uptake.

2.4 Euphotic depths

Irradiance was measured using a 4π downwelling Photosynthetically Available Radiation (PAR) sensor attached to the CTD frame. Euphotic depth was calculated as 1% of surface irradiance.

2.5 Current velocity data

255 The raw east and north components of current velocity down to approximately 300m
256 were measured using a ship-mounted 150 kHz RDI Acoustic Doppler Current Profiler
257 (ADCP) and logged using RD Instruments data acquisition software (DAS version
258 2.48 with profiler firmware 17.20). The instrument was configured to sample over 120
259 second intervals with 96 bins of 4 m thickness, pulse length 4 m and a blank beyond
260 transmit of 4m. Spot gyro heading data were fed into the transducer deck unit where
261 they were incorporated into the individual ping profiles to correct the velocities to
262 earth co-ordinates before being reduced to 2 minute ensembles. Subsequent
263 processing steps merged the ADCP data with corrected heading information for the
264 ship's navigational GPS data-stream to obtain speed and direction, The ship's velocity
265 is also calculated from spot positions taken from the master navigation file and taken
266 from the ADCP velocities, resulting in an absolute water velocity in terms of east-
267 west and north-south velocities, (see Burkill (2006)). Calibration of the 150 kHz
268 ADCP was achieved using bottom tracking data collected after departure from
269 Falmouth while crossing the continental shelf. The calibration involves the application
270 of two corrections; a misalignment angle and an amplitude factor. The misalignment
271 angle (ϕ) corrects for the rotational position of the ADCP on the ships hull relative to
272 the ships axis. The amplitude factor (A) corrects for the fore-aft tilt of the instrument
273 relative to the horizontal plane.
274
275 *2.4 MVP data*
276
277 A fine scale survey of the mesoscale physics and key variables of the upper ocean was
278 conducted using a towed Conductivity, Temperature, Depth (CTD) device known as
279 the Moving Vessel Profiler (MVP). The instrument used was a BOT (Brookes Ocean

Technology) MVP 300 with an AML micro CTD instrument (S/N 7027). During the survey, the MVP was towed behind the ship at a speed of 11-11.5 knots, undulating up and down in the water column and completing a full surface-to-300m depth return profile every 12-13 minutes in which time it travelled 4km. The MVP was towed along a pre-defined survey grid, Figure 1. Application of a temperature lag of $\tau = 0.12$ s was found necessary to account for the delayed response of the temperature sensor. More details can be found in the cruise report (Burkill, 2006). The MVP CTD was calibrated by comparison to data from the surface thermosalinograph (TSG) data, which had in turn been calibrated against data from the frame CTD casts. All MVP temperature and salinity data from between 4 and 5m were extracted and merged with the corrected TSG data. The difference between the MVP and corrected TSG in terms of temperature and salinity was displayed in scatter plots. It was found necessary to apply an offset of -0.033 to salinity but none to temperature.

3. Results

3.1 Turbulent diffusivities

A representative profile for the turbulent diffusivity, κ, is shown in Fig 3a. Despite the averaging of profiles for each deployment there is still considerable variability in mean profiles for κ between deployments. Nevertheless, there are consistent patterns. In the surface layer κ is generally of order 10^{-3} - 10^{-2} m^2 s^{-1}, but occasionally much larger for the shallowest observations. At greater depth κ is of order 10^{-5} - 10^{-4} m^2 s^{-1}. For the daily profiles at the central PAP site the mean depth of the euphotic zone is 50.8 ± 5.7(sd) dbar.

Note that in the density profile shown there is no clear seasonal pycnocline (Figure 3f). This was a feature of several profiles. However, strong agreement was found between density-inferred mixed layer depth and the depth to which mixing was enhanced near the surface over the cruise as a whole (not shown). Fluxes into the mixed layer are not discussed here because there was evidence that substantial production was taking place below the mixed layer (Painter et al., 2008a). Instead we focus on how the turbulent nitrate supply contributes to nitrate uptake throughout the euphotic zone.

It should be noted that the large variability in estimated diffusivities, even at the same depth (note the logarithmic scale), does not indicate that the instrument or technique here is insufficiently precise. Rather it reflects the strongly intermittent nature of turbulence at centimetre to metre scales – something long recognised (e.g. Gregg, 1987; Gibson, 1991; Frisch, 1995).

3.2 Nitrate supply at fixed stations relative to nitrate uptake

Before presenting the estimates of turbulent nitrate flux into the euphotic zone, it is worth making a few comments regarding the other component of the calculation, the vertical profile of nitrate. Figure 3b shows the nitrate vertical profile obtained immediately preceding the turbulence profile in Figure 3a. The gradual increase in nitrate concentration with depth is a standard feature. For all but two of the profiles obtained immediately preceding a turbulence profiler deployment, the surface nitrate concentration is of order 1 mmol N m^{-3}. For the two anomalous profiles, concentrations are still greater than 0.3 mmol N m^{-3}. Therefore it is unlikely that nitrate was limiting phytoplankton growth during the cruise period.

A consequence of the sparse vertical spacing of bottle samples inevitably obtained from CTD casts is that the calculated gradients in the nitrate profile are rather variable (Figure 3c). Furthermore, the small number of points means that smoothing by running averages or interpolating by anything other than a linear method are questionable: smoothing would be certain to move the profile away from the few data points we have for each cast: a higher order interpolation would be very difficult to constrain with any confidence. Although either method would give a smoother nitrate profile, and hence a more regular gradient, it would do so at a cost that is difficult to justify. We also choose to use individual nitrate profiles for the central station rather than the statistical model discussed earlier as they were taken immediately prior to turbulence profiling. It is therefore necessary to accept some variability in gradients. It should be noted that unlike turbulent diffusivity we cannot form error bars accounting for the variability of nitrate profiles as we only have one CTD cast on which nitrate samples were taken for each turbulence station. Therefore the errors in nitrate profiles, gradients and flux are likely to be larger than those indicated in Figures 3, 4 and 5 where only the variability due to turbulent diffusivity is quantified. Fig 3c shows the nitrate gradient for the representative profile. For all casts the gradients are typically 0.1 mmol N m^{-4}. Fig 4 shows the mean and standard deviation for the nitrate gradients calculated using the nitrate profiles obtained on CTD frame casts preceding a turbulence deployment. For the euphotic depth horizon of interest (51m), the mean and standard deviation for the gradient are 0.13 mmol N m^{-4} and 0.06 mmol N m^{-4} respectively.

The nitrate uptake at each depth, once more for the same representative profile, is shown in Figure 3d. There is a general decrease with depth, with a small

maxima (seen in some but not all other casts) around 15m where the turbulent mixing drops sharply (Fig 3a).

Fig 3e shows the turbulent nitrate flux at each depth calculated using equation 2 for the same representative profile. Superimposed on this is the total nitrate uptake integrated to that depth. Note the logarithmic scale. The euphotic depth for this profile is also marked. It is apparent that for this station the turbulent supply of nitrate to the euphotic zone is almost two orders of magnitude smaller than the contemporaneous total uptake of nitrate within it.

Figure 5 demonstrates the consistency in the relationship between uptake and turbulent flux at the central PAP site for the 11 days of the study. The mean uptake rate in the euphotic zone is 5.1+/-1.3 mmol N $m^{-2}d^{-1}$, whilst the mean turbulent flux is 0.09 mmol N $m^{-2}d^{-1}$, with 95% confidence intervals of 0.05 mmol N $m^{-2}d^{-1}$ and 0.16 mmol N $m^{-2}d^{-1}$.

3.3 Estimates of turbulent diffusivity from vertical shear

The relationship of small scale turbulent mixing to the hydrographic properties of stratification and vertical shear has received much attention (e.g. Pacanowski & Philander, 1981; Peters et al., 1988; Turner, 1975; Yu & Schopf, 1997). In particular people have sought to relate the strength of mixing to the Richardson number,

$$Ri = N^2(z)/S^2(z),$$

which represents the competing influences of stratification, as represented by the buoyancy frequency

$$N(z) = \sqrt{\frac{g}{\rho}\frac{\partial \rho}{\partial z}} \quad (3)$$

(where g is the acceleration due to gravity, z is depth and ρ is density), and vertical current shear,

$$S(z) = \frac{\partial |\underline{u}|}{\partial z},$$

(where $\underline{u}$ is the current velocity) in controlling the likely onset of turbulence. We test the ability of three different parameterisations to estimate the turbulent diffusivity for our survey. Velocity profiles from the ADCP are used to estimate S, extracting data simultaneous with the turbulent profiler deployment. We begin by using hydrographic data from the CTD sensors on the turbulence probe to calculate N. Using this estimate for N provides the most direct and hence fairest comparison to our direct measurements of κ. More specifically, N is actually calculated as N^2 from the square of equation (3) using 4 dbar binned data for ρ in order to be consistent with the 4 dbar averaging used for ADCP data and for the MVP data later.

Because the calculation of both N and S require vertical derivatives they, like the nitrate gradient discussed earlier, are sensitive to relatively small distortions in the vertical profile. As data for these are much higher in frequency (every 4 dbar) than for the nitrate profiles, we can justifiably smooth these. A running average of 7 adjacent bins (28 dbar) gives the best match between direct and indirect observations of turbulent diffusivity.

Figure 6 shows the comparison of direct observations to predictions from the (a) Pacanowski and Philander (1981), (b) Yu and Schopf (1997) and (c) Peters, Gregg and Toole (1988) parameterisations. The Pacanowski and Philander (1981) parameterisation (hereafter PP) is the most accurate. Fig 6d demonstrates that between 50m and 200m the PP estimate is generally within a factor of 2 of the direct estimate. Given the large variability in direct estimates, this is perhaps surprisingly good. It

should be noted that a certain amount of serendipity may be involved. PP was developed for a model with a horizontal grid size of 40 km x 70 km and a non-uniform vertical resolution of order 15 km near the surface. Here, however, shear is calculated at 4 m vertical resolution (albeit after applying a moving 28 m, or 7 bin, window average to smooth it first) and the horizontal resolution will typically be between 10 m and 100 m (due to the mounting angle of the ADCP the horizontal scale will be roughly the depth of the measurement). The difference in scales between our data and PP means that a direct 1:1 relationship can not be expected. In particular, the key gradients in vertical velocity and density may be significantly larger at 4 m resolution than that of the Paconowski and Philander (1981) model. Given the results shown in Fig.6, PP is nevertheless adopted as our parameterisation for estimating the diffusive flux of nitrate across the region covered by the mesoscale survey.

It should be noted that the above comparison is the most direct possible. To estimate turbulent fluxes during the mesoscale survey, when κ was not directly measured away from the central station, it is necessary to use hydrographic data from the MVP to estimate N. This data was averaged and smoothed in an identical manner to that applied to the turbulence probe CTD data for consistency. Without a number of direct measurements at other locations within the region it is impossible to quantify any associated change in precision.

3.4 Variability in diffusive nutrient supply across the region

Using MVP CTD data to calculate the buoyancy frequency and simultaneous ADCP data to calculate the shear, we estimated the turbulent diffusivities throughout the mesoscale survey. These estimates were combined with the previously discussed

427 statistical model for the nitrate profile to estimate the associated fluxes of nitrate into
428 the euphotic zone across the region, as shown in Fig 7. The area of each dot is
429 proportional to the flux. The largest flux (3.1 mmol N m^{-3}) is very much larger than
430 the other fluxes so it is not included in the colour scale but is instead solely
431 represented by area. Note that Fig.6 indicates that our parameterisation for turbulent
432 diffusivity may often be in error by a factor of 2. Therefore the fluxes, being linear in
433 turbulent diffusivity carry the same potential error. .

434 Using the median euphotic depth of 48 dbar (estimated from all 28 CTDs casts
435 that comprised the survey), the mean diffusive flux is 0.12 mmol N m^{-2} d^{-1}. The
436 predicted nitrate concentration at this depth is 5 mmol N m^{-3} +/- 1 mmol N $m^{-3.}$ Such a
437 20% potential error is minor compared to those associated with the estimate of the
438 diffusivity. The distribution of fluxes is significantly non-Gaussian with standard
439 deviation of 0.26 mmol N m^{-2} d^{-1}. (There is, at face-value, a single hot-spot at 49.15N
440 16.75W with flux more than 20 times greater than the mean, clearly visible in Figure
441 7. The reliability of this observation is addressed in the Discussion.) Therefore the
442 median value, 0.08 mmol N m^{-2} d^{-1}, is a more representative figure. The euphotic
443 depth is also distributed in a non-Gaussian manner for the region. However, all
444 euphotic depths bar one (an outlier of 100 dbar) are between 40 and 70 dbar. If the
445 calculation is repeated for these depths then the median flux is 0.10 mmol N m^{-2} d^{-1}
446 with 0.10 mmol N m^{-2} d^{-1} standard deviation at 40 dbar and 0.09 mmol N m^{-2} d^{-1} with
447 0.11 mmol N m^{-2} d^{-1} standard deviation at 70 dbar . It is apparent therefore that at
448 these depths the estimate of nitrate flux into the euphotic zone is relatively insensitive
449 to the precise depth used for the calculation. All rates are seen to be close to those
450 estimated directly at the central PAP site in Section 3.1.

The near uniformly low fluxes seen in Figure 7 are consistent with the rather amorphous dynamical structure of the region. Figure 7 also shows potential temperature at 47m to highlight this. There are no strong frontal regions which could lead to enhanced shear either by themselves or via interactions with the wind. (The strong dynamical signature of an eddy in the southwest corner (Painter *et al*., 2008b) only manifests itself below 100m). The cluster of 3 higher fluxes near 49.1^{o}N and 16.7^{o}W are actually in one of the regions with most widely spaced isotherms.

4. Discussion

Our estimates for the turbulent flux of nitrate into the euphotic zone for both the central PAP site and the mesoscale survey are consistent. Both give a value of approximately 0.1 mmol N m^{-2} d^{-1}. It is worth putting this in context with previous studies. Lewis et al. (1986) diagnosed a flux of 0.14 mmol N m^{-2} d^{-1} in the subtropical North Atlantic. Carr et al. (1995) found the flux to be between 0.1 and 1 mmol N m^{-2} d^{-1} between 0 and 2S in the equatorial Pacific but at least an order of magnitude smaller outside this region. In the northern North Atlantic, Law et al., (2001) found a large turbulent flux of 1.8 mmol N m^{-2} d^{-1}, using an SF6 tracer to infer vertical turbulent mixing. Using the same technique in the Southern Ocean they estimated the flux to be an order of magnitude smaller 0.17 mmol N m^{-2} d^{-1}. The discrepancy was due to a substantially smaller inferred turbulent diffusivity in the Antarctic Circumpolar Current. Both of the latter two studies, however, quantified the nitrate flux into the mixed layer rather than into the euphotic zone.

Our direct estimates of the turbulent flux of nitrate into the euphotic zone are one to two orders of magnitude less than the rate of nitrate uptake within it for the

476 same period. This raises the obvious question of what mechanisms supply or supplied
477 the nitrate that was taken up. Over recent years it has become increasingly apparent
478 that physical processes at the mesoscale and submesoscale (Mahadevan & Archer,
479 2000; Levy et al., 2001) can induce very large vertical fluxes, associated for example
480 with the formation and interactions of eddies (McGillicuddy & Robinson, 1997;
481 Martin & Richards, 2001) and with strong frontal regions (Allen et al., 2005; Lapeyre
482 & Klein, 2006). In theory the mesoscale survey would allow the calculation of vertical
483 velocities using the Omega equation (e.g. Pollard and Regier, 1992). However, such a
484 calculation needs to be constrained by the change in distributions between multiple
485 surveys to have any degree of robustness. Consequently we have no such estimates
486 for this cruise. There is also the potential that more nutrient rich water may be
487 advected horizontally into the site. Our dataset does not allow us to quantify such a
488 flux. However, other papers in this volume (Hartman et al; Painter et al. 2008a;
489 Smythe-Wright et al.) present evidence that such nutrient rich incursions do occur.
490 Therefore, here we only compare the rate of uptake to the nitrate flux associated with
491 convective mixing the previous winter. We stress that this is a rather crude analysis
492 purely intended to determine the likely relative magnitude of fluxes.
493 The CTD profiles for the surveyed region are curious since they show no clear
494 signal of winter mixing, taking such a signal to be a region of homogeneous
495 hydrographic properties below the seasonal thermocline. This is true whether one
496 examines temperature, salinity, density or oxygen. We therefore turn to the Coriolis
497 Project (http://www.coriolis.eu.org/) for information on winter mixed layer depths.
498 This database stores CTD profiles from ARGOS floats, gliders, buoys, moorings and
499 standard ship CTD casts. We have extracted temperature data (as this is the only
500 parameter recorded by all available profiles) for an approximately 200kmx200km

501 square centred on the PAP site for the period 1 February to 30 June 2006. Figure 8
502 shows the mixed layer depths for this period, calculated using a criterion of a decrease
503 in temperature of 0.05ºC with respect to that at 5m depth. This is somewhat smaller
504 than has been used by others (e.g. Oka et al. (2007) use 0.2^{o}C). However, individual
505 examination of potential temperature profiles indicated that this criterion gave the
506 most accurate diagnosis of mixed layer depth for the period studied, using the
507 criterion of matching the base of the deep winter homogenous layer. The maximum
508 mean monthly mixed layer depth is in February, extending to approximately 350 m
509 with one profile showing a 400 m mixed layer. These estimates for winter mixed layer
510 depth are consistent with climatological data from the World Ocean Atlas
511 (http://www.cdc.noaa.gov/cdc/data.nodc.woa94.html; Antonov et al., 2006; Locarnini
512 et al. 2006) which reports a mean February mixed layer depth for the same area
513 between 277 m and 472 m. We therefore take a representative value of 400m,
514 acknowledging that this might result in a small overestimate. From the deeper profiles
515 obtained during our cruise we know that the nitrate concentration at this depth is
516 approximately 10.5 mmol N m^{-3}. Using the simplest approach of multiplying nitrate
517 concentration at the base of the winter mixed layer by the euphotic depth, winter
518 mixing to 400m would therefore have provided a stock of approximately 504 mmol N
519 m^{-2} within the euphotic zone (mean euphotic depth of 48dbar * 10.5 mmol N m^{-3}).
520 Unfortunately, oxygen profiles were not available to utilise the 'oxygen step' method
521 of Koeve (2001). After subtracting the 127 mmol N m^{-2} still present above the
522 euphotic depth during the cruise, this leaves approximately 75 days supply at the
523 mean nitrate uptake rate of 5 mmol N m^{-2} d^{-1}. Therefore, if nitrate uptake was roughly
524 the same for the 75 days preceding the start of the cruise (at the end of June) then
525 deep winter mixing would have to extend into mid-April to provide sufficient stocks

526 by itself. Except for two points (discussed below), the observations from mid-March
527 onwards reveal a mixed layer depth that is no deeper than the euphotic depth during
528 the cruise (Figure 8). Therefore, without sporadic deeper mixing between mid-March
529 and June, another mechanism must provide sufficient nitrate to the euphotic zone both
530 to match the observed uptake and to give the observed residual nitrate stock of 127
531 mmol N m^{-2}. There are two anomalously deep mixed layer depths later in the year. If
532 the temperature profile for the second of these (on Julian day 140) is examined more
533 closely there is evidence of a warming in the top few metres which has been missed
534 by the simple criterion used here. Hence the mixed layer is arguably much shallower
535 than the norm rather than deeper. However, the first anomalous point (on Julian day
536 130) has a homogenous profile to nearly 100m. This apparent deep mixing event
537 would deliver a substantial extra flux of nitrate to the mixed layer. We assume, once
538 again, that nitrate uptake has been constantly 5 mmol N m^{-2} d^{-1}. There would,
539 therefore, remain, by Julian day 130, 229 mmol N m^{-3} of the nitrate entrained into the
540 euphotic zone by winter mixing. We also assume that the concentration at greater
541 depths remains at 10.5 mmol m^{-3} on Julian day 130. Mixing to 99m, as the
542 observation suggests, would consequently introduce an extra 158 mmol N m^{-2} to the
543 euphotic zone. This is sufficient for an extra 31 days at the uptake rate of 5 mmol N
544 m^{-2} d^{-1}. Such an event would therefore allow deep winter mixing to meet the uptake
545 requirements given the above assumptions. However, nitrate uptake is likely to have
546 been much larger earlier in the year, during the spring (unless Fe-limited; see Moore
547 et al. (2006)). Consequently it is still most probable that another significant nitrate
548 source is required to close the budget, especially as our estimate of winter mixing
549 using the nitrate concentration at the base of the winter mixed layer may be an over-
550 estimate by as much as 50% (Koeve, 2001). The cumulative 9.5 mmol N m^{-2} that

551 would result from extrapolation of our estimates for the diffusive supply over the
552 same period (from mid-March to the end of June) is forty-fold smaller than the flux
553 due to convective mixing even if convection stopped in mid-March. Hence, turbulent
554 mixing will only have been a minor contribution.

555 In the absence of nitrate uptake data throughout the year, especially the spring,
556 it is impossible to put a firm estimate on the nitrate flux being delivered by pathways
557 other than winter convective mixing and small-scale turbulent mixing. Furthermore,
558 the 127 mmol N m^{-2} remaining in the euphotic zone at the end of the cruise would
559 only have lasted roughly 25 days at the observed uptake rate. The missing flux needs
560 to be of equivalent magnitude to the excess nitrate uptake taking place during the
561 spring period plus whatever nitrate would be utilised from the middle of August to the
562 end of the year.

563 To put the diffusive flux in a broader context, recent estimates for the rate of
564 nitrification in the euphotic zone in the North Atlantic indicate a typical value of 0.01
565 mmol N m^{-3} d^{-1} (D.Clark, pers.comm.; C.Fernandez I., pers.comm.). Integrating over
566 the euphotic depth gives a nitrification flux of almost 0.5 mmol N $m^{-2}d^{-1}$. This is five
567 times larger than the turbulent flux of nitrate reported here. It should, however, be
568 noted that there is a great deal of variability in measurements of nitrification (Yool et
569 al., 2007). Nevertheless, extant observations indicate that nitrification might be an
570 equivalent, if not larger, flux of nitrate to the euphotic zone than turbulent mixing in
571 mid / late summer for the studied area.

572 By 'validating' the most effective parameterisation for our area we have
573 estimated the variability in turbulent nitrate flux across a roughly 100 km x 100 km
574 region centred on the PAP site. There was remarkably little variability, especially
575 given the inherently variable nature of turbulent mixing. The one 'hot-spot'

576 (highlighted in Section 3.4) is instructive in the care needed for estimating turbulent
577 nutrient fluxes. The flux at this location is the largest measured in the area by some
578 margin and represents an extreme outlier. By looking at the vertical profiles for shear
579 and buoyancy frequency (not shown) it is possible to determine that it is due to small
580 deviations in shear and buoyancy frequency that may have been removed by a more
581 aggressive smoothing. This reinforces the care needed in using parameterisations of κ.
582 Inevitably subjective choices on the degree of smoothing exert a major influence on
583 the resulting estimates. For this reason, the results on variability presented here should
584 only be viewed as preliminary and individual fluxes, particularly outlying ones,
585 should be treated with care. Future fieldwork should ensure that profiles of turbulent
586 diffusivity and nitrate are obtained at a number of different locations within a region
587 as an independent check on the indirect method. In particular profiles should be
588 sought in differing physical regimes, covering a range of shear and buoyancy
589 frequency. There is little evidence of strong shear layers in the data collected by this
590 cruise, despite the presence of an eddy in the southeast corner of the surveyed region
591 (Painter et al., 2008b). Nevertheless, shear is often found to be significantly enhanced
592 in the vicinity of strong mesoscale features such as eddies and fronts (Allen & Smeed,
593 1996). The need for extra direct observations covering a range of regimes is therefore
594 even more vital in a strong dynamical region, where theory suggests the turbulent flux
595 may be more significant.
596
597 **5. Conclusions**
598
599 We have presented results on both direct and indirect estimates of the nitrate flux due
600 to vertical turbulent mixing for the PAP site and its environs. Comparison of the direct

estimates to simultaneous nitrate uptake measurements indicates that the turbulent flux is a small contributor to the nitrate budget at the PAP site. A rough calculation suggests that winter mixing is a major contributor. A simple analysis, however, indicates that other mechanisms, most likely related to mesoscale physical phenomena, may be equally significant.

We have also 'validated' a parameterisation for indirect estimation of turbulent mixing and used this to estimate the nitrate flux into the euphotic zone throughout the survey region. These indirect estimates agree with direct estimates in terms of magnitude. They also vary very little across the region.

Acknowledgements

We would like to thank Jon Sharples and Mark Moore for useful discussions regarding the processing of turbulent diffusivity data, Alberto Naveira-Garabato for advice on the application and limitations of parameterisations for turbulent mixing, Robin Hankin for his statistical expertise and finally, but most definitely not least, the captain and crew of RRS Discovery for providing such a superb platform for oceanographic research. This manuscript contributes to NOCS Theme 2 of the Oceans 2025 core programme funded by the Natural Environmental Research Council, UK. Adrian Martin was also part funded by an NERC Advanced Research Fellowship (NER/J/S/2001/00708).

References

625 Allen, J. T., Brown, L., Sanders, R., Moore, C.M., Mustard, A., Fielding, S., Lucas,
626 M., Rixen, M., Savidge, G., Henson, S., Mayor, D. 2005. Diatom carbon export
627 enhanced by silicate upwelling in the northeast Atlantic. Nature 437, 728-732.
628
629 Allen, J.T., Smeed, D.A., 1996. Potential Vorticity and Vertical Velocity at the
630 Iceland-Færœs Front. Journal of Physical Oceanography 26, 2611–2634
631
632 Antonov, J. I., R. A. Locarnini, T. P. Boyer, A. V. Mishonov, and H. E. Garcia, 2006.
633 World Ocean Atlas 2005, Volume 2: Salinity. S. Levitus, Ed. NOAA Atlas NESDIS
634 62, U.S. Government Printing Office, Washington, D.C., 182 pp.
635
636 Baker, M. A., Gibson, C. H., 1987. Sampling turbulence in the stratified ocean:
637 statistical consequences of strong intermittency. Journal of Physical Oceanography
638 17, 1817-1836.
639
640 Burkill, P.H., 2006. RRS Discovery Cruise 306, 23 Jun - 6 Jul 2006. Pelagic
641 biogeochemistry of the PAP site. Cruise Report No. 9. National Oceanography Centre,
642 Southampton, UK.
643
644 Carr, M.-E., Lewis, M.R., Kelley, D., Jones, B., 1995. A physical estimate of new
645 production in the equatorial Pacific along 150ºW. Limnology and Oceanography 40,
646 138-147.
647
648 Dugdale, R.C., Goering, J.J., 1967. Uptake of new and regenerated forms of nitrogen
649 in primary production. Limnology and Oceanography 12, 196-206.

650

651 Dugdale, RC., Wilkerson, FP., 1986. The use of ^{15}N to measure nitrogen uptake in
652 eutrophic oceans; experimental considerations. Limnology and Oceanography 31, 673-
653 689.

654

655 Frisch, U., 1995. Turbulence, Cambridge University Press, 310 pages.

656

657 Gibson, C.H., 1991. Turbulence, mixing, and heat flux in the ocean main thermocline.
658 Journal of Geophysical Research 96, 20403-20420.

659

660 Gregg, M.C., 1987. Diapycnal Mixing in the Thermocline: A Review. Journal of
661 Geophysical Research 92, 5249-5286.

662

663 Jenkins, W. J., Doney, S.C., 2003. The subtropical nutrient spiral. Global
664 Biogeochemical Cycles 17, 1110, doi:10.1029/2003GB002085.

665

666 Kirkwood, D.S., 1996. Nutrients: practical notes on their determination in seawater.
667 ICES Techniques in Marine Environmental Sciences Report 17. International Council
668 for the Exploration of the Seas, Copenhagen, 25pp. ISSN 0903-2606.

669

670 Koeve, W., 2001. Wintertime nutrients in the North Atlantic – new approaches and
671 implications for new production estimates. Marine Chemistry 74, 245-260.

672

673 Lapeyre, G., Klein, P., 2006. Impact of the small-scale elongated filaments on the
674 oceanic vertical pump. Journal of Marine Research 64, 835-851.

675

676 Law, C. S., Martin, A. P., Liddicoat, M. I., Watson, A. J., Richards, K. J., Woodward,
677 E. M. S., 2001. A Lagrangian SF6 tracer study of an anticyclonic eddy in the North
678 Atlantic: patch evolution, vertical mixing and nutrient supply to the mixed layer.
679 Deep-Sea Research II 48, 705-724.

680

681 Law, C.S., Abraham, E.R., Watson, A.J., Liddicoat, M.I., 2003. Vertical eddy
682 diffusion and nutrient supply to the surface mixed layer of the Antarctic Circumpolar
683 Current. Journal of Geophysical Research 108, doi: 10.1029/2002JC001604.

684

685 Ledwell J.R., Watson, A.J., Law, C.S., 1998. Mixing of a tracer in the pycnocline.
686 Journal of Geophysical Research, 103, 21,499–421,529.
687 Lewis, M.R., Harrison, W.G., Oakley, N.S., Hebert,D., Platt, T. 1986. Vertical nitrate
688 fluxes in the oligotrophic ocean. Science 234, 870-873.

689

690 Levy, M., Klein, P., Treguier, A.-M., 2001. Impact of sub-mesoscale physics on
691 production and subduction of phytoplankton in an oligotrophic regime. Journal of
692 Marine Research 59, 535-565.

693

694 Locarnini, R. A., A. V. Mishonov, J. I. Antonov, T. P. Boyer, and H. E. Garcia, 2006.
695 World Ocean Atlas 2005, Volume 1: Temperature. S. Levitus, Ed. NOAA Atlas
696 NESDIS 61, U.S. Government Printing Office, Washington, D.C., 182 pp.

697

Mahadevan, A, Archer, D., 2000. Modeling the Impact of Fronts and Mesoscale Circulation on the Nutrient Supply and Biogeochemistry of the Upper Ocean. Journal of Geophysical Research 105, 1209-1225.

Martin, A.P., Richards, K.J., 2001. Mechanisms for vertical nutrient transport within a North Atlantic mesoscale eddy. Deep-Sea Research II, 48, 757-773.

McGillicuddy, D.J., Robinson, A.R., 1997. Eddy-induced nutrient supply and new production in the Sargasso Sea. Deep-Sea Research I 44, 1427-1450

Moore, C.M., Mills, M.M., Milne, A., Langlois, R., Achterberg, E.P., Lochte, K., La Roche, J., Geider, R.J., 2006. Iron limits primary productivity during spring bloom development in the central North Atlantic. Global Change Biology 12, 626-634

Naveira-Garabato, A.C., Strass, V., Kattner, G. 2002. Fluxes of nutrients in a three-dimensional meander structure of the Antarctic Polar Front. Deep-Sea Research II 49, 3771-3792.

Osborn, T.R., 1980. Estimates of the local rate of vertical diffusion from dissipation measurements. Journal of Physical Oceanography 10, 83-89.

Pacanowski, R. C., Philander, S. G. H., 1981. Parameterization of vertical mixing in numerical models of tropical oceans. Journal of Physical Oceanography 11, 1443-1451.

723 Painter, S.C., Lucas, M., Stinchcombe, M.C., Bibby, T.S., Poulton, A.J., 2008a.
724 Summertime trends in pelagic biogeochemistry in the NE Atlantic: the PAP site 49N
725 16.5W. Submitted to Deep-Sea Research II.
726
727 Painter, S.C., Pidcock, R., Allen, J.T., 2008b. Mesoscale eddies driving spatial and
728 temporal heterogeneity in the productivity of the euphotic zone of the NE Atlantic.
729 Submitted to Deep-Sea Research II.
730
731 Peters, H., Gregg, M. C., Toole, J. M., 1988. On the parameterization of equatorial
732 turbulence. Journal of Geophysical Research 93, 1199-1218.
733
734 Pollard, R.T., Regier, L.A., 1992. Vorticity and vertical circulation at an ocean front.
735 Journal of Physical Oceanography 22, 609-624.
736
737 Polzin K.L., Toole, J.M., Ledwell, J.R., Schmitt, R.W., 1997. Spatial variability of
738 turbulent mixing in the abyssal ocean. Science 276, 93–96.
739
740 Prandke, H.,2005. Microstructure sensors. In: Marine Turbulence –Theories,
741 Observations and Models. Baumert, Simpson, Sündermann (editors), Cambridge
742 University Press, 101-108.
743
744 Prandke, H., K. Holtsch and A. Stips, 2000. MITEC Report Technical Note No.
745 I.96.87, European Commission, Joint Research Centre, Space Applications Institute,
746 Ispra/Italy.
747
748 Press, W.H., Flannery, B., Teukolsky, S.A., Vetterling, W.T., 1992. Numerical
749 Recipes in FORTRAN 77: The Art of Scientific Computing, 2nd edition. Cambridge
750 University Press. 992 pages.
751

752 Sakamoto, C.M., Johnson, K.S., Coletti, L.J., 2008. An improved algorithm for the
753 computation of nitrate concentrations in seawater using an in situ ultraviolet
754 spectrophotometer. Limnology and Oceanography, in press.
755
756 Sanders, R., Morris, P., Stinchcombe, M., Seeyave, S., Venables, H., Lucas M., 2007.
757 New production and the F ratio around the Crozet Plateau in austral summer 2004-
758 2005 diagnosed from seasonal changes in organic nutrient levels. Deep Sea Research
759 II, doi:10.1016/j.dsr2.2007.06.06
760
761 Turner, J.S. 1973. Buoyancy Effects in Fluids, Cambridge University Press.
762
763 Williams, R.G., McLaren, A., Follows, M.J. 2000. Estimating the convective supply
764 of nitrate and implied variability in export production. Global Biogeochemical Cyles
765 14, 1299-1313.
766
767 Yool, A., Martin, A.P., Fernandez, C., Clark, D., 2007. The significance of
768 nitrification for oceanic new production. Nature 447, 999-1002.
769 (doi:10.1038/nature05885)
770
771 Yu, Z., Schopf, P. S., 1997. Vertical eddy mixing in the tropical upper ocean: its
772 influence on zonal currents. Journal of Physical Oceanography 27, 1447-1458.

773 **FIGURE CAPTIONS**

774

775 **Figure 1.**

776 Map showing the survey track for the cruise. The central PAP site is at 49º50'N

777 16º30'W.

778

779 **Figure 2.**

780 (a) Variation of 'nitrate' (NO3+NO2) concentration versus pressure using data from

781 all profiles taken during the cruise (dots). The solid line shows the predicted nitrate

782 concentration using the fitted model, $N_{pred}=AP^B/(C+P^B)$ where A= 14.5135 mmol N

783 m^{-3}, B= 1.1131 and C= 143.1686 $(dbar)^B$. (b) Actual versus predicted nitrate

784 concentrations (dots) with 1:1 line superimposed. The correlation has R^2=0.91. Units

785 are mmol N m^{-3} for both plots.

786

787 **Figure 3.**

788 Various profiles versus depth for a representative station on year day 179: (a)

789 turbulent diffusivity with mean for station as solid line and 95% confidence limits as

790 dashed lines; (b) 'nitrate' (actually NO3+NO2); (c) nitrate gradient; (d) nitrate uptake;

791 (e) nitrate flux at each depth (mean thin solid line and 95% confidence intervals as

792 dashed) plus cumulative nitrate uptake integrated from surface (thick solid line) and

793 euphotic depth (horizontal solid line) calculated as 1% of surface irradiance; (f)

794 potential density.

795

796 **Figure 4.**

797 Mean (solid) and mean +/- one standard deviation (dashed) profiles of nitrate gradient
798 from CTD frame casts at central PAP site.
799
800 **Figure 5.**
801 Time series of flux and uptake at the central PAP site covering year days 179-187 (28
802 June to 6 July 2007). Turbulent nitrate flux at base of euphotic zone (48m) as thin
803 solid line with 95% confidence interval as dashed lines. Nitrate uptake integrated from
804 surface to base of euphotic depth (determined as 1% surface irradiance for each
805 profile independently) as thick solid line. Note the logarithmic y axis and that no
806 uptake data are available for year day 183.
807
808 **Figure 6**
809 Direct observations of turbulent diffusivity versus estimates from the
810 parameterisations of (a) Pacanowski and Philander (1981), (b) Yu and Schopf (1997)
811 and (c) Peters, Gregg and Toole (1988). The solid line is 1:1 and the dashed lines
812 indicate ¼, ½, 2 and 4 times the 1:1 relationship. (d) shows the fractional difference
813 versus depth between the direct observations and the best parameterisation (PP).
814
815 **Figure 7**
816 Variability in the turbulent flux of nitrate (in mmol N m^{-2} d^{-1}) at the base of the mean
817 euphotic depth (48m) across the mesoscale survey region. The area of each dot (with
818 one for each CTD profile provided by the MVP) is proportional to the corresponding
819 flux. The greyscale also indicates the flux but it is chosen to fit all but the largest flux
820 (3.1 mmol N m^{-2} d^{-1}) for clarity. The dashed lines mark contours of potential
821 temperature to indicate the dynamical physical processes influencing this depth.

822

823 **Figure 8**

824 Mixed layer depth versus year day for a period in 2006. The most consistent criterion
825 for estimating mixed layer depth was found to be the depth at which the temperature
826 is 0.05 lower than at 5m depth. The hydrographic data is a combination of profiles
827 from ARGOS floats and gliders and is taken from the Coriolis database
828 (http://www.coriolis.eu.org/). Also shown as a solid line is the mean euphotic depth
829 for the cruise discussed here.

830

831

832

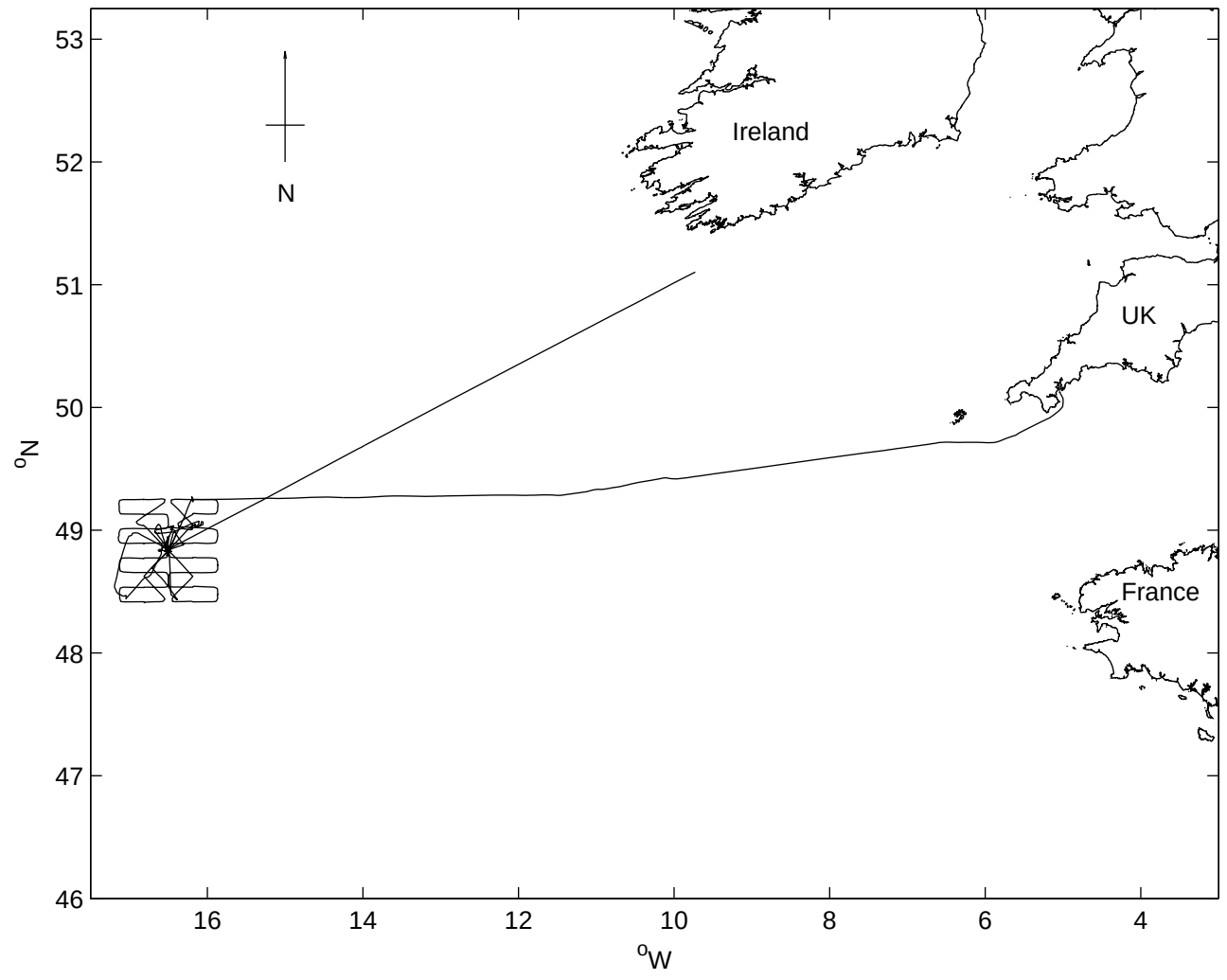
Ireland
UK
France
N
53
52
51
50
49
48
47
46
°N
16
14
12
10
8
6
4
°W

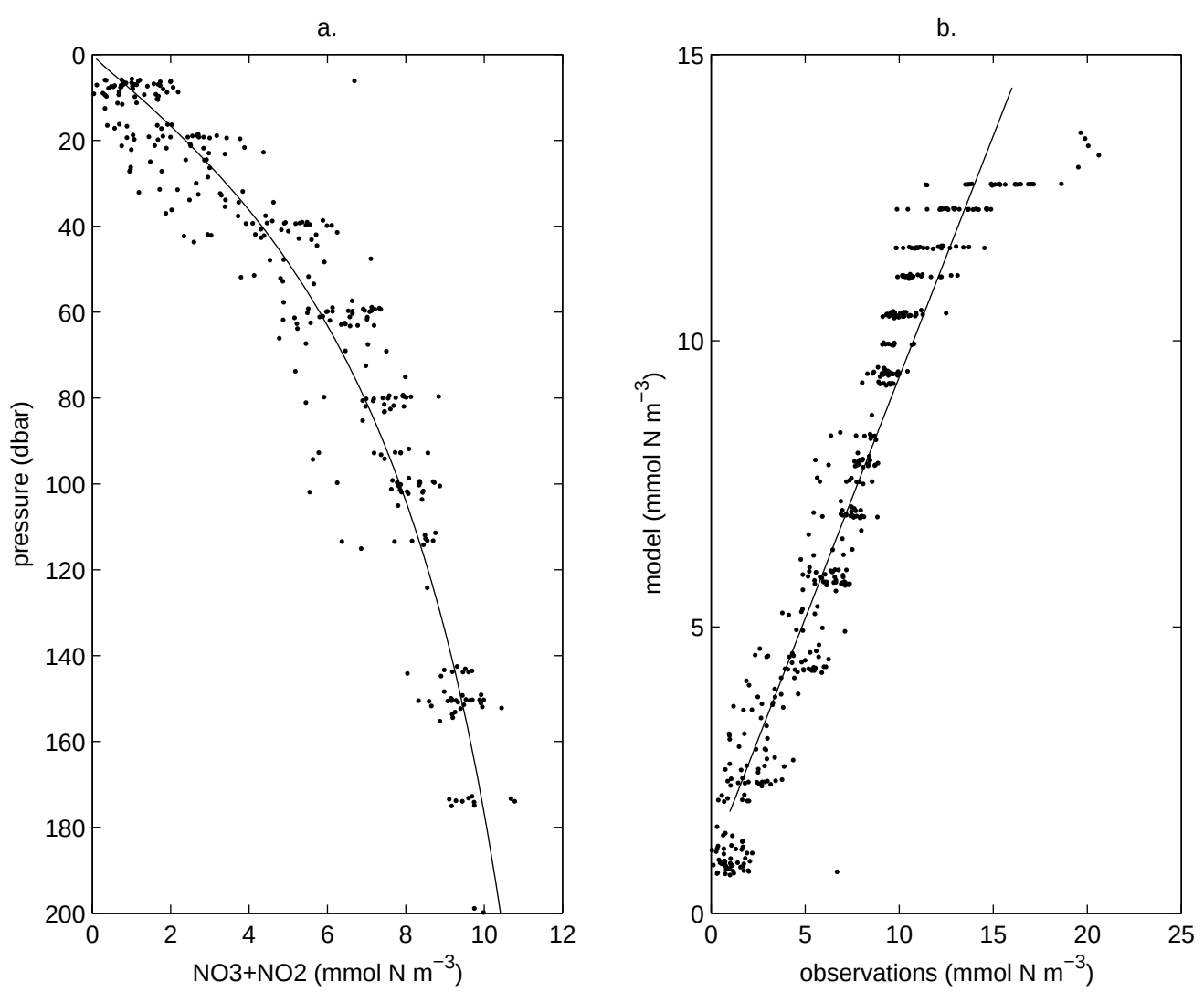
a.
b.
pressure (dbar)
NO3+NO2 (mmol N m^{-3})
model (mmol N m^{-3})
observations (mmol N m^{-3})
0
20
40
60
80
100
120
140
160
180
200
0
2
4
6
8
10
12
15
10
5
0
0
5
10
15
20
25

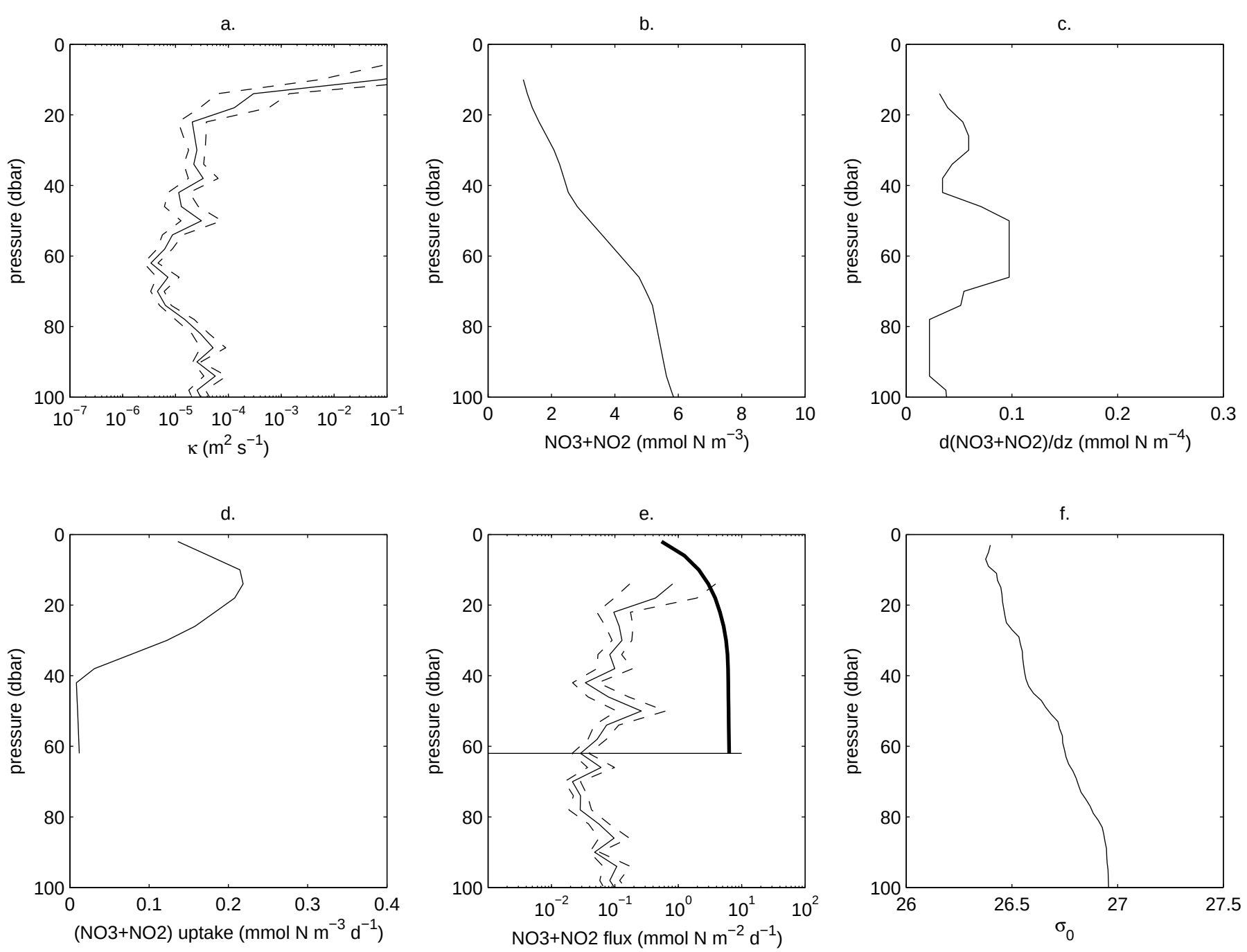
a.
b.
c.
d.
e.
f.
pressure (dbar)
κ (m2 s−1)
NO3+NO2 (mmol N m−3)
d(NO3+NO2)/dz (mmol N m−4)
(NO3+NO2) uptake (mmol N m−3 d−1)
NO3+NO2 flux (mmol N m−2 d−1)
σ0

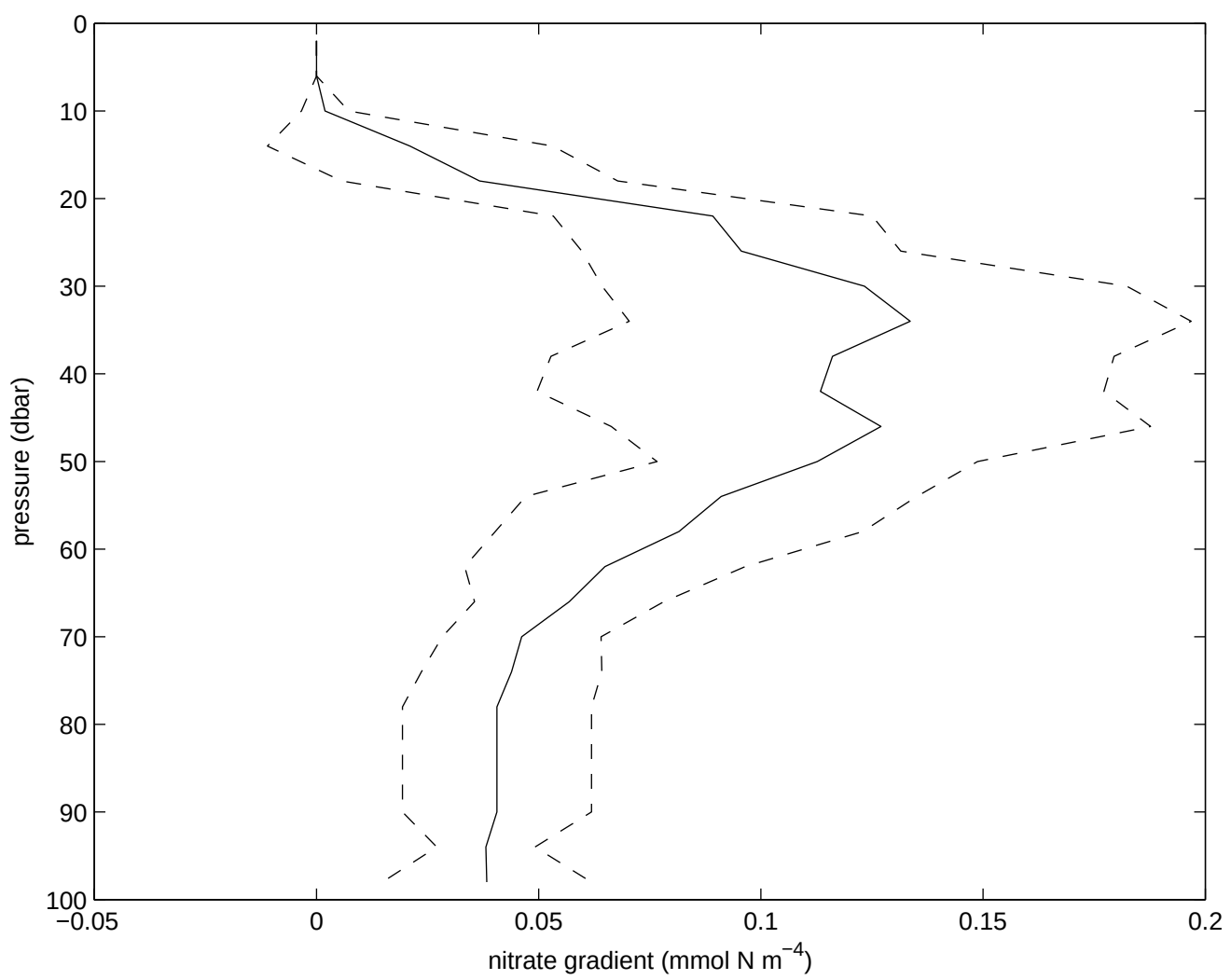
0
10
20
30
40
50
60
70
80
90
100
pressure (dbar)
−0.05
0
0.05
0.1
0.15
0.2
nitrate gradient (mmol N m^{-4})

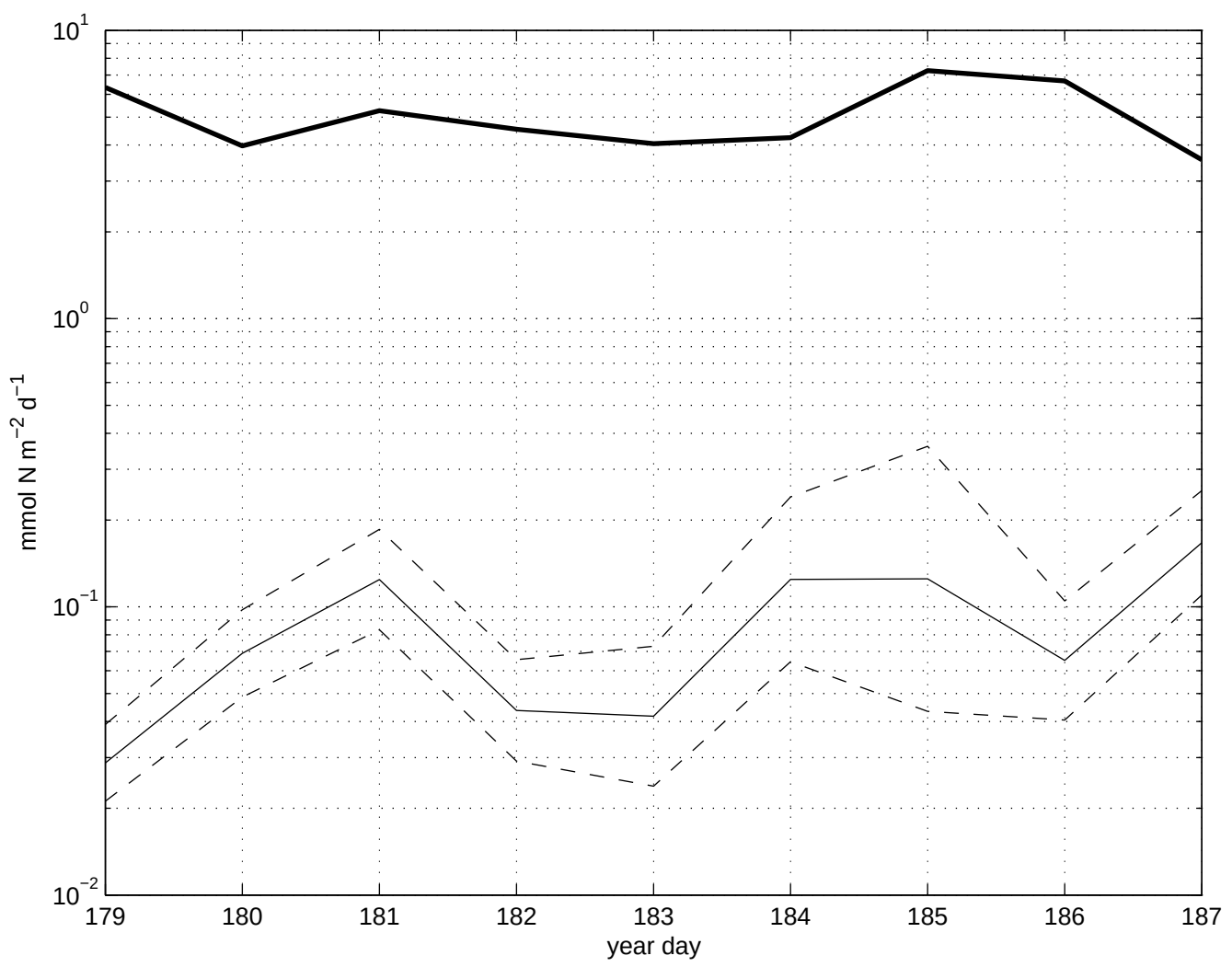
10^{1}
10^{0}
10^{-1}
10^{-2}
mmol N m^{-2} d^{-1}
179
180
181
182
183
184
185
186
187
year day

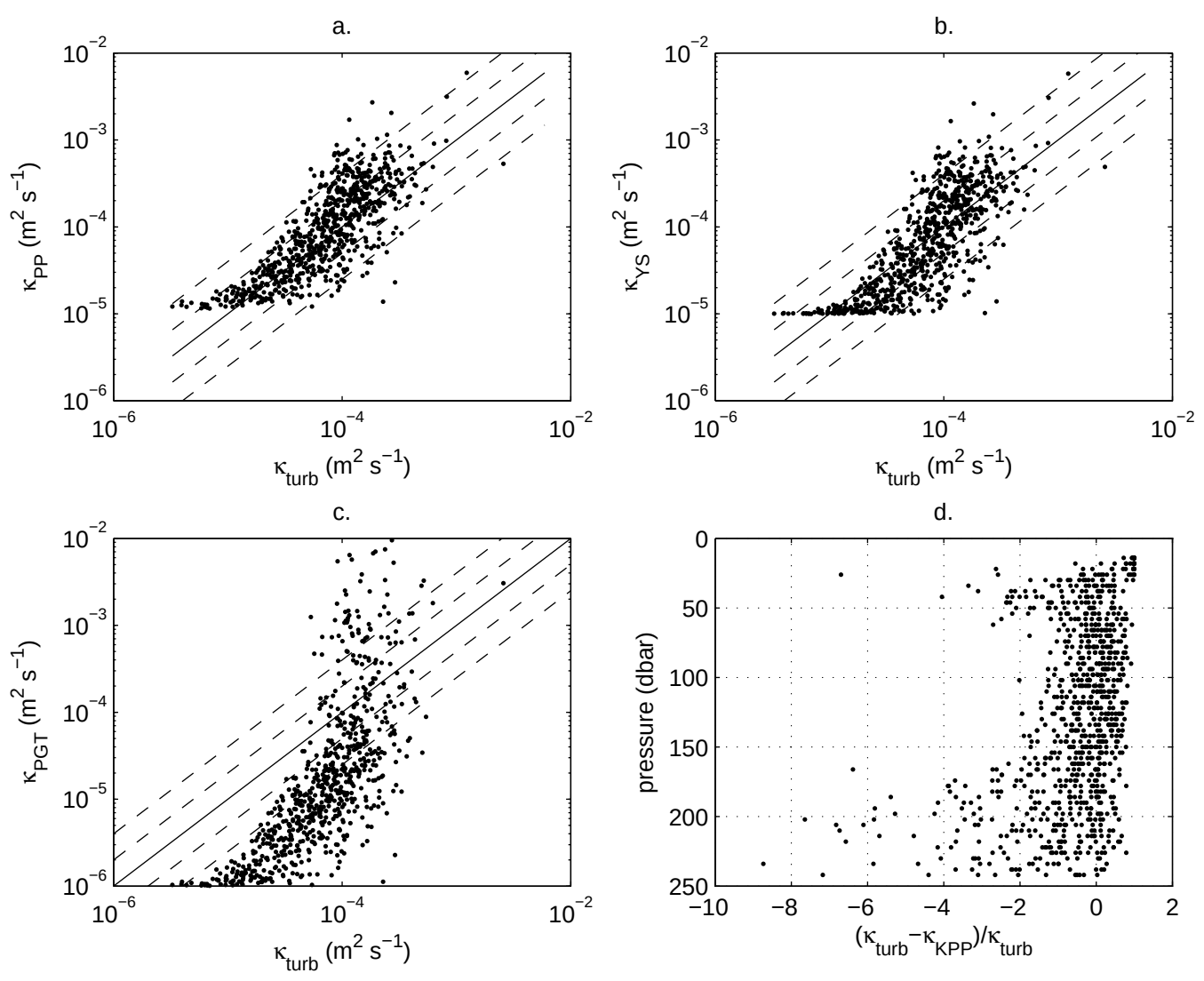
a.
b.
c.
d.
κ_{PP} (m^2 s^{-1})
κ_{YS} (m^2 s^{-1})
κ_{PGT} (m^2 s^{-1})
κ_{turb} (m^2 s^{-1})
pressure (dbar)
$(\kappa_{turb}-\kappa_{KPP})/\kappa_{turb}$

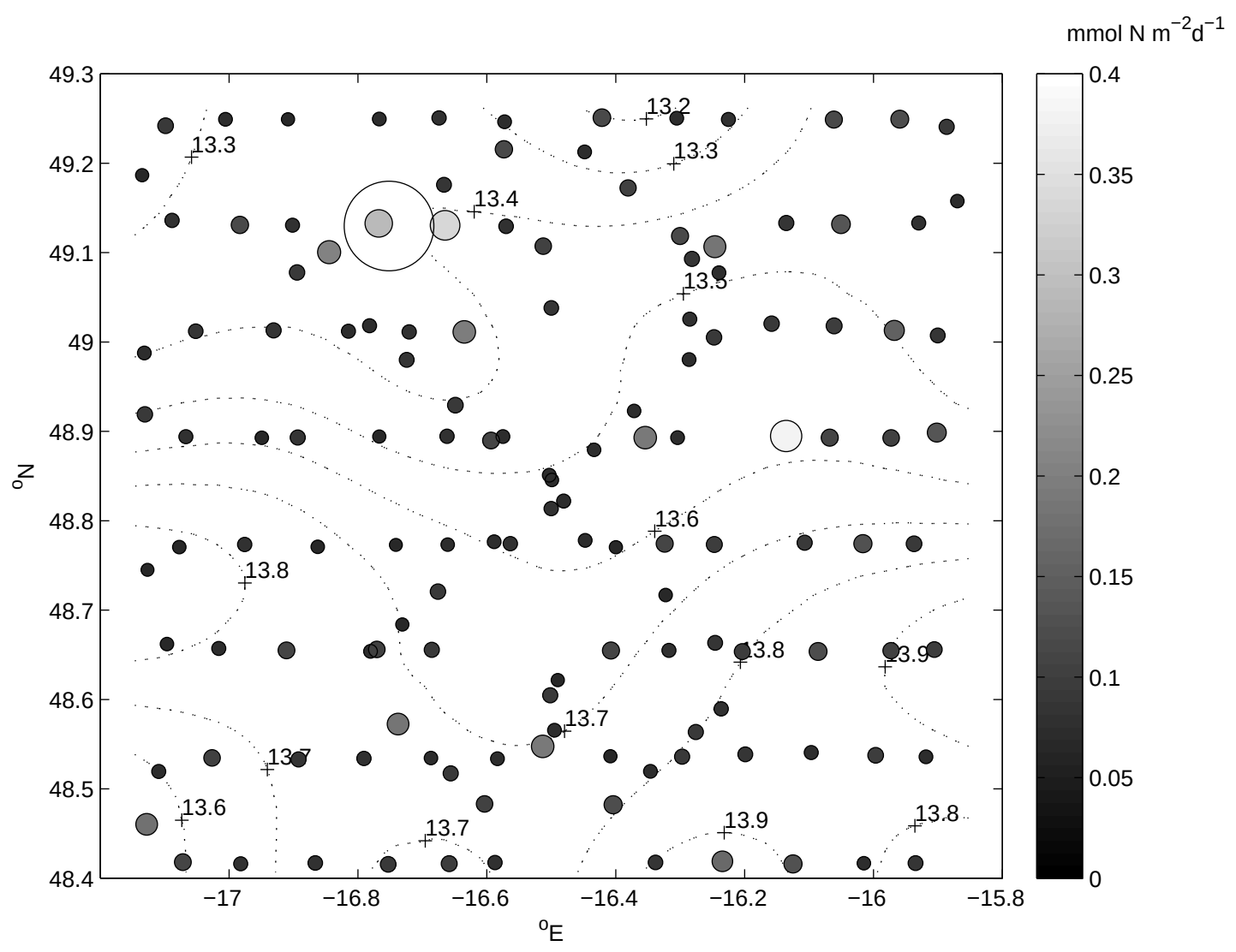
mmol N m^{-2}d^{-1}
0.4
0.35
0.3
0.25
0.2
0.15
0.1
0.05
0
49.3
49.2
49.1
49
48.9
48.8
48.7
48.6
48.5
48.4
^{o}N
−17
−16.8
−16.6
−16.4
−16.2
−16
−15.8
^{o}E
13.2
13.3
13.3
13.4
13.5
13.6
13.8
13.8
13.9
13.7
13.7
13.6
13.7
13.9
13.8

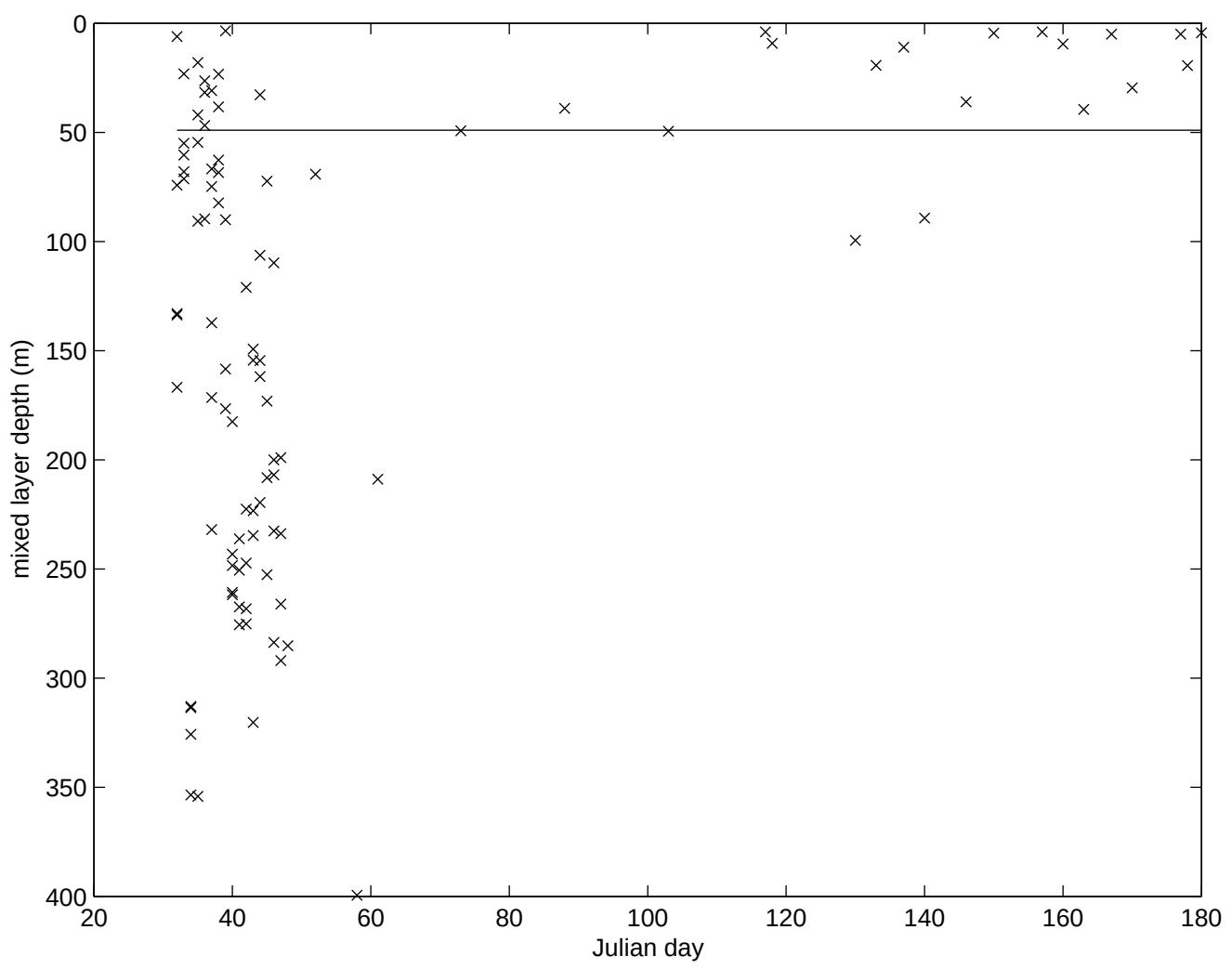
0
50
100
150
200
250
300
350
400
mixed layer depth (m)
20
40
60
80
100
120
140
160
180
Julian day